



# Hot Corrosion Performance of AlO-CrO/Ni-CoCrAlYT<sub>a</sub> and AlO/NiCoCrAlYT<sub>a</sub> Coatings Deposited by Atmospheric Plasma Spraying

Chong Tao, Lei Wang, Nailiang Cheng, Hengfa Hu, Yang Liu, and Xiu Song

(Submitted August 20, 2015; in revised form February 15, 2016)

AlO-CrO/NiCoCrAlYT<sub>a</sub> and AlO/NiCoCrAlYT<sub>a</sub> coatings were deposited on 316L stainless steel substrate using atmospheric plasma spraying, respectively, in order to improve the oxidation and corrosion resistance. The hot corrosion performance of the coatings at 700 and 900 °C were studied, and the detailed microstructures and phase composition of the coatings were analyzed using x-ray diffraction, scanning electron microscope with energy dispersive spectrometer, and transmission electron microscope. The results show that both coatings are structurally featured by slatted layers, consisting of amorphous phase, Cr<sub>2</sub>O<sub>3</sub>, Ni<sub>3</sub>Al, and Al<sub>2</sub>O<sub>3</sub>. The hot corrosion resistance of AlO-CrO/NiCoCrAlYT<sub>a</sub> coating is better than that of AlO/NiCoCrAlYT<sub>a</sub> coating. This improvement is attributed to lower porosity and more compact Cr<sub>2</sub>O<sub>3</sub> in AlO-CrO/NiCoCrAlYT<sub>a</sub> coating which performs better than Al<sub>2</sub>O<sub>3</sub> in blocking further inward progress of corrosion and oxidization.

**Keywords** APS, coating, hot corrosion, MCrAlY

## 1. Introduction

With the development of industrial appliances, many hot components have endured more severe service environment with higher temperature and complex atmosphere. So, the hot corrosion resistance of these materials should be further improved. Nowadays, making coating, as one of the effective methods to protect base material, has gained more attentions and has been widely used in actual industry. Among the available thermal spraying methods, atmospheric plasma spraying (APS), as a flexible and versatile technology, has been developed recently. During APS, powder materials are firstly heated to a molten or semi-molten state, and then deposited onto the substrate to form a dense and uniform coating. For example, the Al<sub>2</sub>O<sub>3</sub> and Cr<sub>2</sub>O<sub>3</sub> coatings as the representative of oxide ceramic coatings have been widely used in modern industry and exhibit good mechanical and anti-wear performances (Ref 1).

**Chong Tao** and **Hengfa Hu**, Key Laboratory for Anisotropy and Texture of Materials (Ministry of Education), Northeastern University, Shenyang 110819, China and Baosteel Group Shanghai Meishan Iron & Steel Co. LTD, Shanghai, China; **Lei Wang**, **Yang Liu**, and **Xiu Song**, Key Laboratory for Anisotropy and Texture of Materials (Ministry of Education), Northeastern University, Shenyang 110819, China; and **Nailiang Cheng**, Baosteel Group Shanghai Meishan Iron & Steel Co. LTD, Shanghai, China. Contact e-mails: 83708945@qq.com and wanglei@mail.neu.edu.cn.

Moreover, it has been reported (Ref 2-5) that the MCrAlY-based coating in which M is Ni, Co, or Ta, has performed a good resistance to oxidation and corrosion at high temperature, and good properties including plasticity and thermal fatigue strength. In addition, the MCrAlY-based coating has a little effect on the mechanical properties of substrates. Some experts have reported that MCrAlY-based coatings exhibit better high-temperature oxidation and hot corrosion resistance than others, such as NiCoCrAlYSiB coatings (Ref 6, 7) The addition of silicon to the coatings is beneficial to improve both high-temperature oxidation and hot corrosion resistance (Ref 8-11).

However, few researches have been presented regarding the detailed microstructures and corrosion properties of NiCoCrAlYT<sub>a</sub> coating with the addition of Al<sub>2</sub>O<sub>3</sub> and Cr<sub>2</sub>O<sub>3</sub> by APS. In the present study, microstructures and corrosion behavior of APS sprayed AlO-CrO/NiCoCrAlYT<sub>a</sub> and AlO/NiCoCrAlYT<sub>a</sub> coatings were investigated, and the mechanism was also discussed.

## 2. Experimental Procedure

### 2.1 Materials and APS Thermal Spraying Process

The coatings on a stainless steel 316L substrate were prepared by APS. Three commercially available feedstock powders Al<sub>2</sub>O<sub>3</sub>, Cr<sub>2</sub>O<sub>3</sub>, and NiCoCrAlYT<sub>a</sub> with the purity of above 99.5% were used.

Figure 1 shows the morphologies of these powders with a particle size range of 15-45 μm. Before the coating process, 20 mm × 20 mm × 10 mm specimens were cut from stainless steel 316L and were degreased and grit blasted to get a roughness of about 15 μm. Then the coatings were obtained with the abovementioned powders

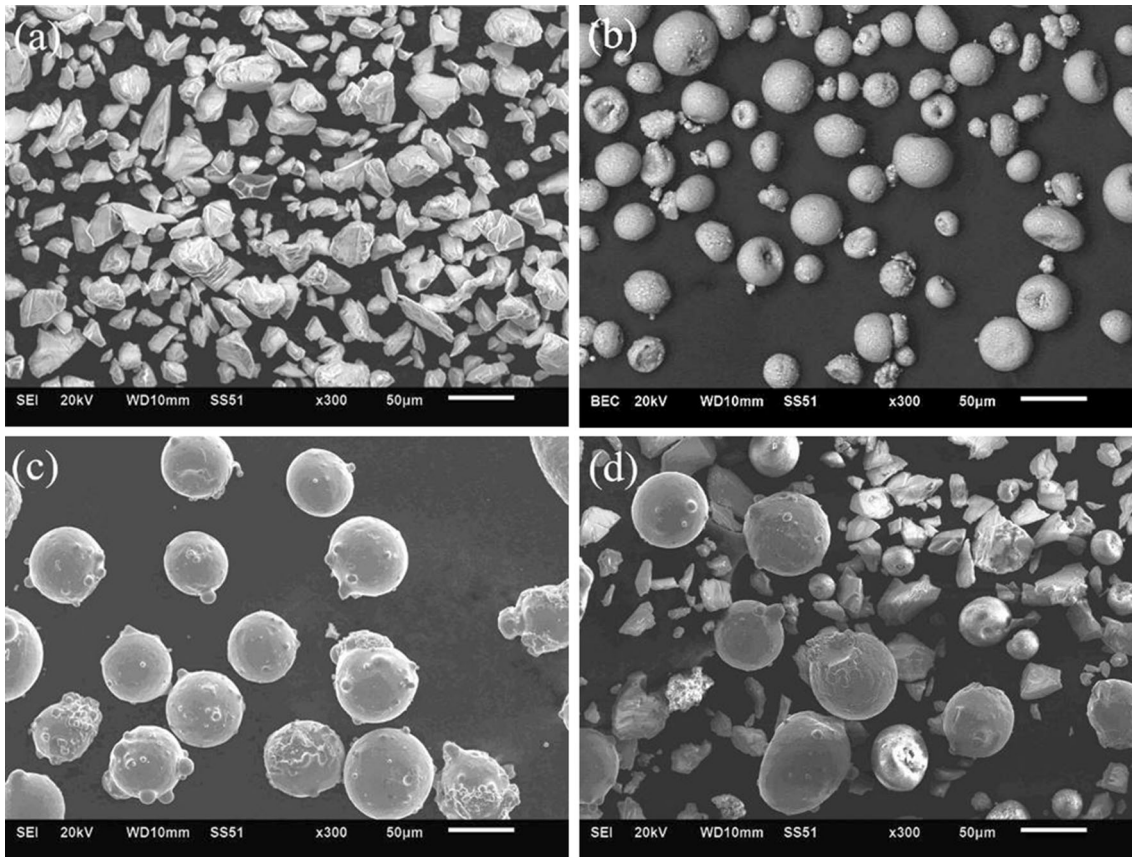


**Fig. 1** The spherical morphologies of the powders: (a)  $\text{Al}_2\text{O}_3$ , (b)  $\text{Cr}_2\text{O}_3$ , (c) NiCoCrAlYTa, (d) mixed powders

**Table 1** Powder ratio of coating samples (mass%)

Samples	Ratio		
	$\text{Al}_2\text{O}_3$	$\text{Cr}_2\text{O}_3$	NiCoCrAlYTa
C1	18	12	70
C2	30	0	70

using a commercial APS (Praxair Surface Technology Model 3710 Plasma, USA), and the torch model is SG-100. Spraying processes were executed with a stand-off distance of 80 mm at a voltage of 40 V and a current of 500 A. The powder feed rate was fixed at 45 g/min with the aid of a computerized powder feeder station. The flow rates of primary Ar gas and secondary He gas were 55 and 18 L/min, respectively. The thickness of the coatings deposited was of  $180 \pm 20 \mu\text{m}$  after 6 passes of the spray gun.

In order to assess the influences of  $\text{Cr}_2\text{O}_3$  content on hot corrosion of composite coatings, two coatings namely C1 and C2 were prepared (Table 1). The Vickers' micro-hardness of the coating and the substrate was tested by the method of indentation. The microstructures of the coatings were characterized using x-ray diffraction (XRD Bruker D8-Advanced German), scanning electron microscope (SEM JEOL 6510A Japan), and transmission electron microscope (TEM FEI Tecnai G<sup>2</sup> 20 USA). The hardness of

coatings was measured using digital micro-hardness tester (DMT SMTMF MHV2000 China) on the cross-section of specimens at every 50  $\mu\text{m}$  from the top to the substrate.

## 2.2 Hot Corrosion Test

Hot corrosion tests were performed in a chamber furnace at 700 and 900 °C in the air, respectively, by soaking in molten salt (75 mass%  $\text{Na}_2\text{SO}_4$  + 25 mass% NaCl) with the purity of above 99%. The furnace (SRJX-8-13) with the KSY-12 controller and the K-Type thermocouples was used. The specimens were completely immersed in the  $\text{Al}_2\text{O}_3$  crucible filled with about 30 g molten salt and retrieved at regular intervals of 5 h. They were washed in hot water at about 90 °C for 10 min, to remove the remaining salt from the specimens' surface. After drying in an air oven at 100 °C for 20 min, they were weighted using the analytical balance with a precision of  $10^{-4}$  g. After mass measurement, the specimens were re-immersed in fresh salts to repeat the above processes. The total time of hot corrosion test was 50 h. The experiment with each condition was repeated using three specimens. The rate of weight gain  $\Delta w_i$  was calculated using Eq 1:

$$\Delta w_i = \frac{w_i - w_0}{A} \quad (\text{Eq 1})$$

where  $i$  is the corrosion cycle number;  $w_i$  is the weight of samples after each corrosion cycle; and  $w_0$  is the initial

weight of samples *A* is the area of sample. Hot corrosion kinetics curves of mass changing with time were made after finishing hot corrosion tests. The surface morphologies of the coatings before and after hot corrosion tests were analyzed using SEM.

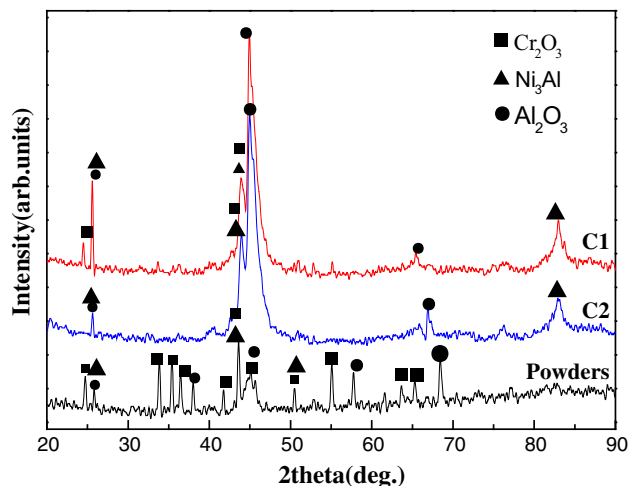


**Fig. 2** XRD patterns of the feedstock powder and as-sprayed coating

### 3. Results and Discussion

#### 3.1 Phase Composition

XRD patterns of the feedstock powder and as-sprayed coatings are shown in Fig. 2. It is clear that  $\text{Cr}_2\text{O}_3$ ,  $\text{Ni}_3\text{Al}$ , and  $\text{Al}_2\text{O}_3$  are detected in the feedstock powder. It is also obvious that there is a distinct diffuse diffraction peak around  $2\theta \approx 45^\circ$ , indicating the formation of an amorphous/nanocrystallized phase during the APS process due to particle melting and high cooling rate during deposition. The similar phase has also been mentioned by earlier reports in other APS coatings (Ref 12-14). Compared with C2, C1 coating contains much more amount of  $\text{Cr}_2\text{O}_3$ .

#### 3.2 Characterization of the Coatings

The cross-sectional microstructures of as-sprayed coatings are shown in Fig. 3. It reveals that both the two coatings show a fine structure and have a good adhesion to the substrate. The thickness of coatings is about  $180 \pm 20 \mu\text{m}$ . It is also found that the coatings present a lamella structure almost paralleling to the interface between the coating and the substrate. Besides, some melted or semi-melted particles and micro-cracks are observed, which is caused by high velocity spray and high melting point of the powders, indicating that not all the particles are melted during the process. When they are deposited on the substrate and cooled

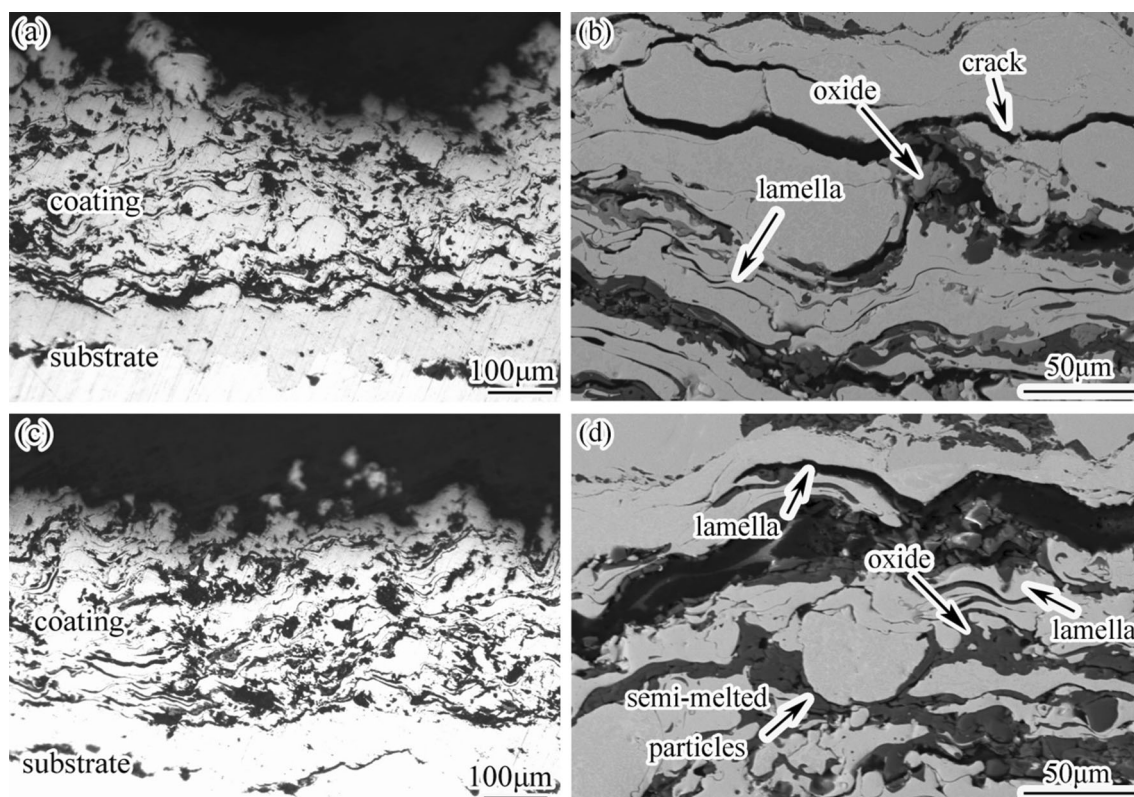


**Fig. 3** Images of cross sections of as-sprayed coatings: (a) OM and (b) SEM of  $\text{Al}_2\text{O}_3\text{-Cr}_2\text{O}_3/\text{NiCoCrAlYTa}$  coating; (c) OM and (d) SEM of  $\text{Al}_2\text{O}_3/\text{NiCoCrAlYTa}$  coating

**Table 2 Powder type and characteristics of testing coatings**

Coating	Feedstock composition	Substrate (HV <sub>0.1</sub> )	Coating hardness (HV <sub>0.1</sub> )	Porosity ratio (%)
C1	AlO-CrO/NiCoCrAlYTa	198	413	15.06
C2	AlO/NiCoCrAlYTa	201	381	17.88

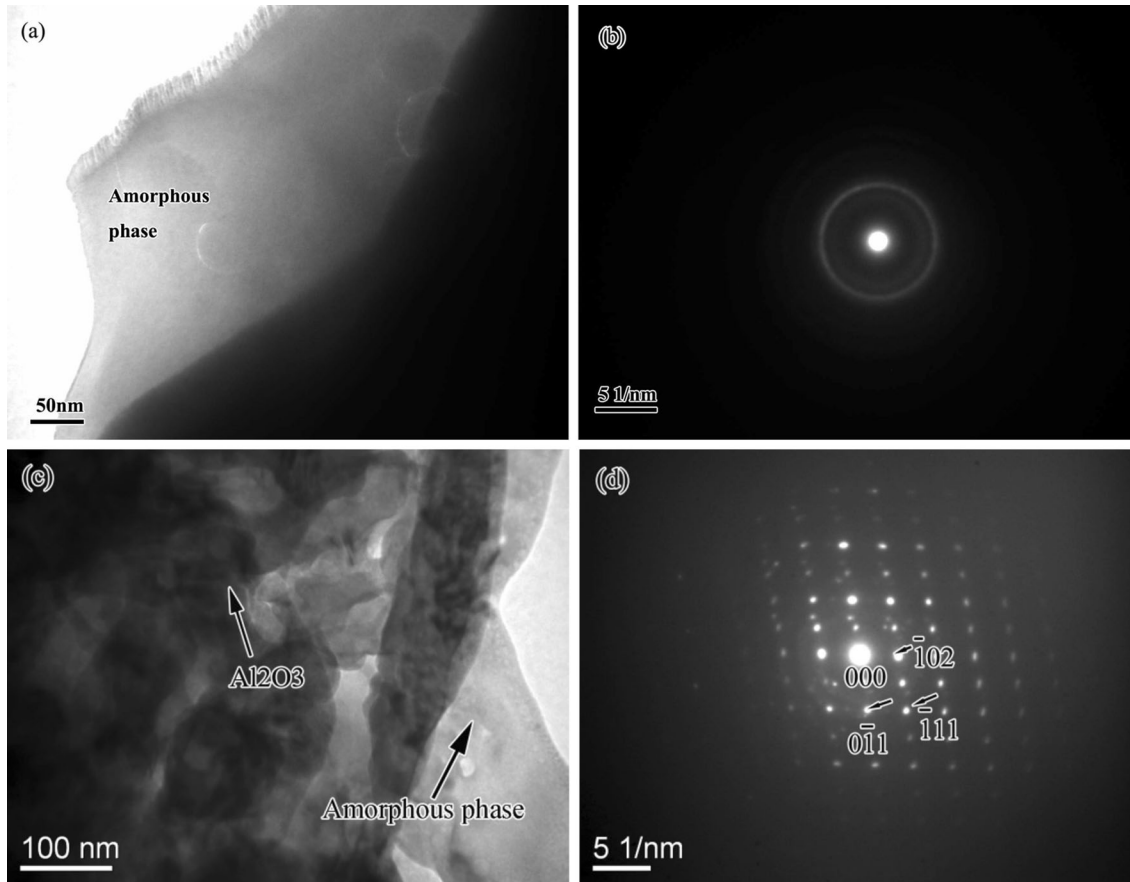


**Fig. 4** TEM images of typical microstructure of coatings: (a) amorphous phase in C1; (b) SAED pattern of amorphous phase; (c) Al<sub>2</sub>O<sub>3</sub> and amorphous phase in C2; (d) SAED pattern of Al<sub>2</sub>O<sub>3</sub>

down, the cracks are generated (Ref 15, 16). Some gray oxides around the splats are showed in Fig. 3, as previously reported by Azarmi et al. (Ref 17).

Table 2 shows the properties of the two kinds of coatings. It indicates that the average porosity of the C1 and C2 coatings is 15.06 and 17.88%, respectively, measured by the image analysis software. And the average micro-hardness is 413HV<sub>0.1</sub> and 381HV<sub>0.1</sub>, respectively, which is approximately as 2 times as that of the substrate (200 HV<sub>0.1</sub>). The enhancement of the surface hardness ascribes to the hard ceramic phases in the coatings. And the higher hardness value of C1 might be due to much more amount of Cr<sub>2</sub>O<sub>3</sub> which is spherical and make it lower porosity than C2.

The typical bright field TEM images of C1 coatings are shown in Fig. 4(a), indicating the coexistence of amorphous phase. Corresponding SAED pattern of amorphous phase (indicated by circle) is shown in Fig. 4(b). The Al<sub>2</sub>O<sub>3</sub> and amorphous phase are found in C2 (Fig. 4c, d).

The partial amorphization of the coating is also evident from the XRD spectra (Fig. 2). Usually, the MCrAlY-based alloy system satisfies the three empirical rules proposed by Inoue et al. (Ref 18), i.e., (1) multi-component, (2) significant atomic size mismatches, and (3) suitable negative heats of mixing among the constituent elements. It is generally known that the glass formation is strongly determined by the atomic radius and mixing enthalpy (Ref 18). In this research, the effective addition of Ni, Co, Cr, Al, Y, and Ta causes the sequential change in the atomic radius in the order of Y (2.27 Å) > Ta (2.09 Å) > Cr (1.85 Å) > Al (1.82 Å) > Co (1.67 Å) > Ni (1.62 Å) (Ref 19), leading to the formation of the packed local structure with low atomic diffusivity in the super cooled liquid (Ref 20). The topological structure and chemical short-range order result from the large negative heated mixing among the constituent elements (Ref 21). In addition, the cooling rate of the splats is

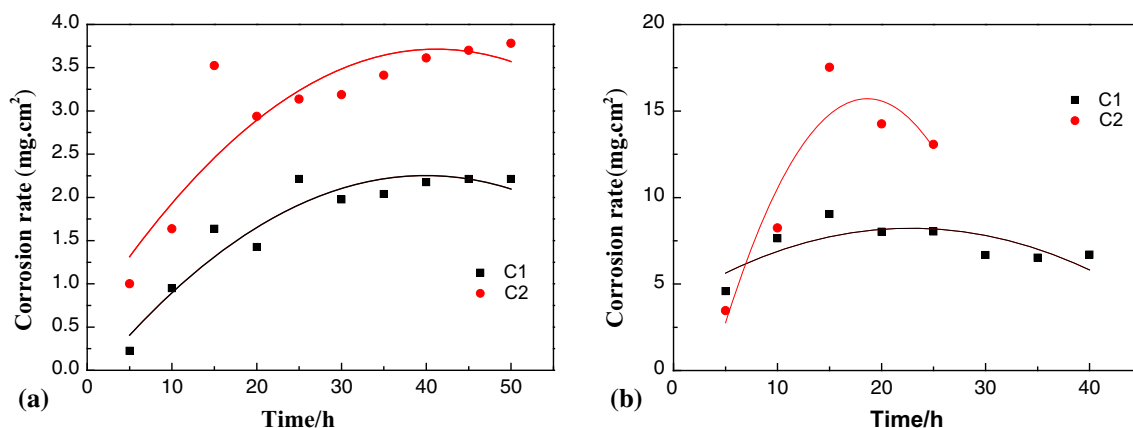


**Fig. 5** Hot corrosion kinetics curves of C1 and C2 coatings at 700 °C (a) and at 900 °C (b)

estimated to be above  $10^6$  K/s during APS processes (Ref 22), which is beneficial to form an amorphous phase.

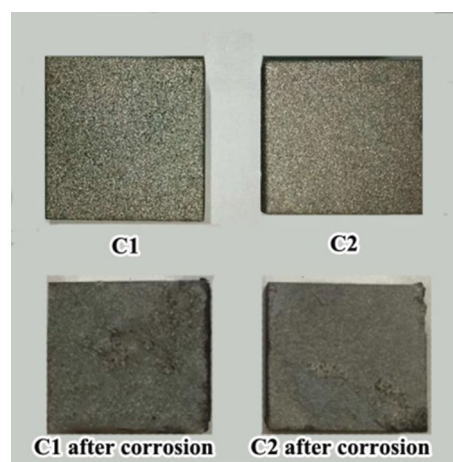
### 3.3 Hot Corrosion Resistance of the Coatings

Hot corrosion kinetics curves of C1 and C2 coatings at 700 °C are shown in Fig. 5(a). At first 25 h, the hot corrosion kinetics curves of C1 and C2 sharply increase. After 25 h, the curves of C1 show a steady state, but the curves of C2 still rises. Figure 5(b) shows the corrosion rate of the C1 and C2 coating at 900 °C for 40 h. It is evident that the corrosion rate of both samples varies with time. The corrosion rate of the C2 coating sample increases within 15 h, then decreases sharply; however C2 coating cracks at 25 h. The corrosion rate of the C1 coating sample rises during first 15 h and then slowly declines. The corrosion kinetic curves incline rapidly in the initial period, because there is no dense and protective oxide film formed on the coating surface yet, and the reaction of oxidation is violent on the surface which is exposed to corrosive medium. In order to simulate the real combustion condition in appliances, the service life of the MCrAl coatings were found to be over 1000 h with the salt spraying method as reported by Nicholls. (Ref 23, 24) However, it is apparent that both C1 and C2 coatings were eroded seriously after 50 h in the salt immersion method, indicating that the higher the salt concentration, the faster the corrosion rate is.

Based on the results in Fig. 5, it is also clear that the corrosion rate of C1 is lower than that of C2 both at 700 and 900 °C. The hot corrosion resistance of C1 is improved by 1.5-2 times compared with that of C2.

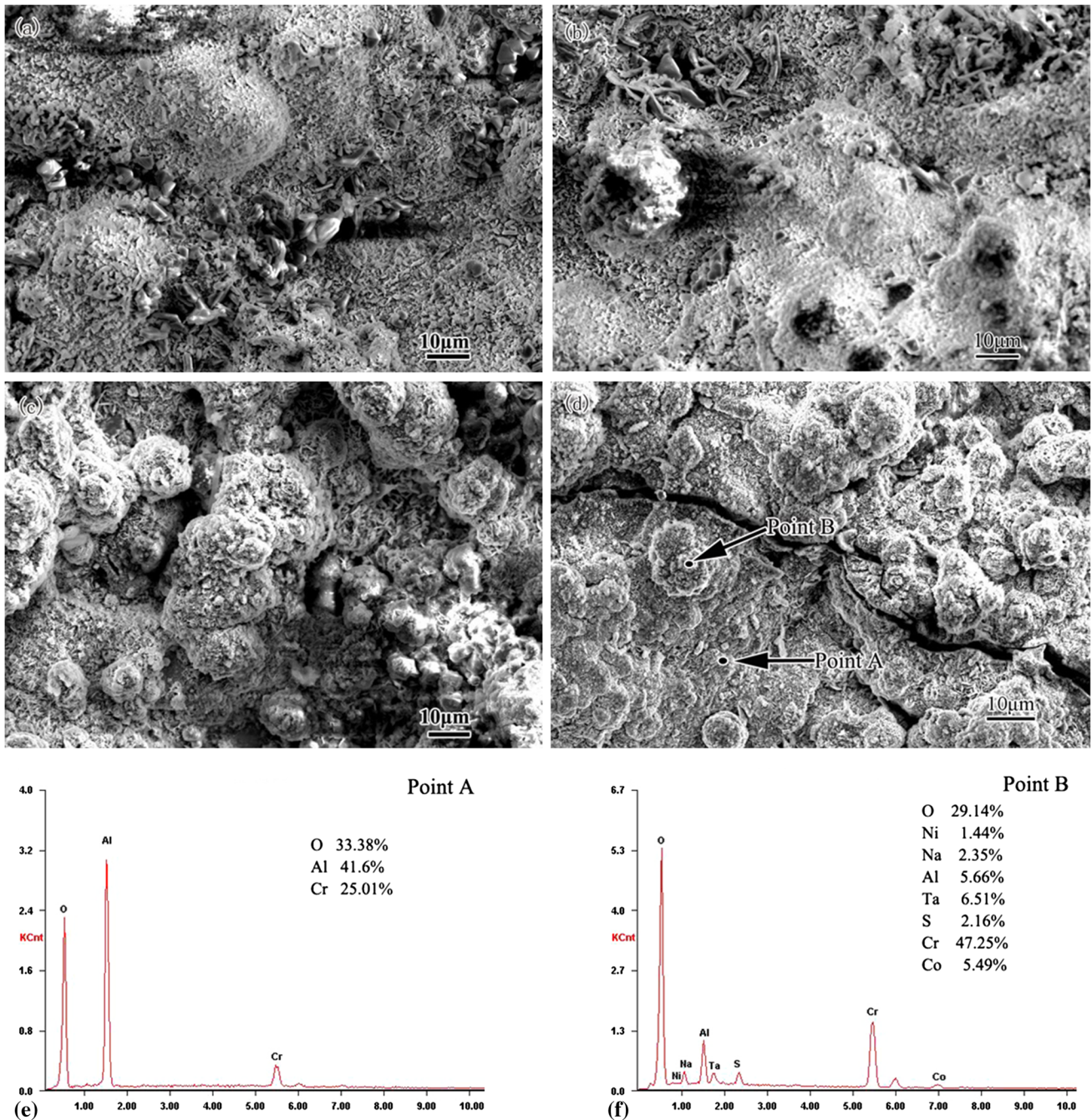
Figure 6 shows outer surface morphologies of C1 and C2 coatings before and after corrosion tests. The dense oxides are seen on the surface, while the oxides on the C2 coating show green in color, indicating that the composition of the oxides is different from each other. In particular, exfoliation can be found on both of them after hot corrosion tests for 50 h. All the above observations are consistent with the corrosion kinetics shown in Fig. 5.

Figure 7 shows the compact oxide film on the coating surface after corrosion. It can be seen that some kinds of



**Fig. 6** Outer surface of the specimens before and after hot corrosion for 50 h

corrosion products are globular and granular generated on the most region of coating surface and they are  $\text{Al}_2\text{O}_3$ ,  $\text{NaCr}_2\text{O}_4$ , and  $\text{Cr}_2\text{O}_3$  detected by XRD (Fig. 8). The surface morphologies of coatings after corrosion at 700 and 900 °C are obviously different. At 700 °C, the corrosion products are mainly globular which are distributed relatively densely on the surface. There are not any obvious holes and cracks on the coating surface. From the SEM images (Fig. 7a, b), it can be seen that the globular corrosion products are many flakes about 3 microns in diameter, while the corrosion products at 900 °C are mainly granular with a diameter of 5-20 microns, as shown in Fig. 7(c) and (d). Meanwhile, many holes and micro-cracks are found on the coating surface. The quantitative EDS analysis on the coating surface after corrosion for 50 h at both A and B points is shown in Fig. 7(e) and (f), respectively. The EDS spectrum of point A reveals that the elements mainly contain O, Al, and Cr, indicating the formation of  $\text{Al}_2\text{O}_3$  and  $\text{Cr}_2\text{O}_3$ . The corrosion products of points B which are globular contain O, Ni, Na, Al, Ta, S, Cr, and Co, suggesting the presence of other oxides.



**Fig. 7** Surface morphologies of C1 (a) and C2 (b) coatings corroded at 700°C, C1 (c) and C2 (d) at 900 °C covered with 75%Na<sub>2</sub>SO<sub>4</sub>+25% NaCl for 50 h and the corresponding EDS spectra (e) and (f)

The cross-sections of as-sprayed coatings after corrosion in molten salt at 700°C are shown in Fig. 9. From Fig. 9(a), it can be seen that there are some micro-cracks between C1 coating and substrate after corrosion for 15 h, because of the formation of corrosion products. And the cracks do not propagate and the C1 coating keeps a good adhesion to the substrate after 50 h as shown in Fig. 9(b). From Fig. 9(c), it can be seen that the structure of C2 is similar to that of C1, and some micro-cracks exist between

coating and substrate. Figure 9(d) shows the structure of C2 after corrosion in molten salt for 50 h, indicating that the cracks have a mass propagation. The cracks are parallel to the interface between coating and substrate which would lead the coating to spall from the substrate.

Al<sub>2</sub>O<sub>3</sub> and Cr<sub>2</sub>O<sub>3</sub> are formed in both APS process and hot corrosion process (Ref 25, 26), when the Cr/Al mass ratio is more than 4, otherwise, Al<sub>2</sub>O<sub>3</sub> is mainly formed when the Cr/Al mass ratio is less than 4 (Ref 27). In the

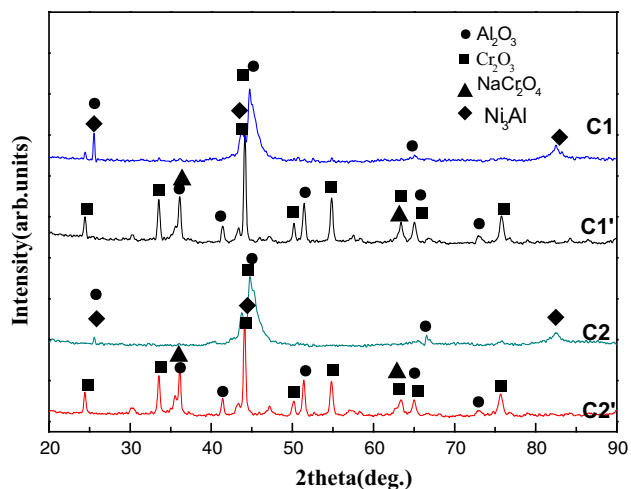


**Fig. 8** XRD pattern of C1 and C2, C1', and C2' after corrosion in molten salt at 700 °C

present research, the Cr/Al mass ratios of C1 and C2 coatings are 2/1 and 17/19, respectively, less than 4, so Al<sub>2</sub>O<sub>3</sub> is mainly produced.

When the samples were put in hot-melt solution of 75%Na<sub>2</sub>SO<sub>4</sub>+25%NaCl for 5 h, the coatings were isolated from the outside air. Because the solubility and diffusion velocity of oxygen in molten salt is limited, the supply of oxygen mainly relies on the decomposition of Na<sub>2</sub>SO<sub>4</sub>. The reaction sequence (Ref 28) is as follows:



At the beginning of the hot corrosion, Al<sub>2</sub>O<sub>3</sub> film quickly forms on the coating surface. Then it dissolves in the neutral Na<sub>2</sub>SO<sub>4</sub> where chemical reactions take place. The formation of oxides on the coating surface reduces the oxygen activity in molten salt, increasing the sulfur activity. Sulfur diffuses to the substrate through the oxide film and forms sulfide there. Owing to the diffusion of S into

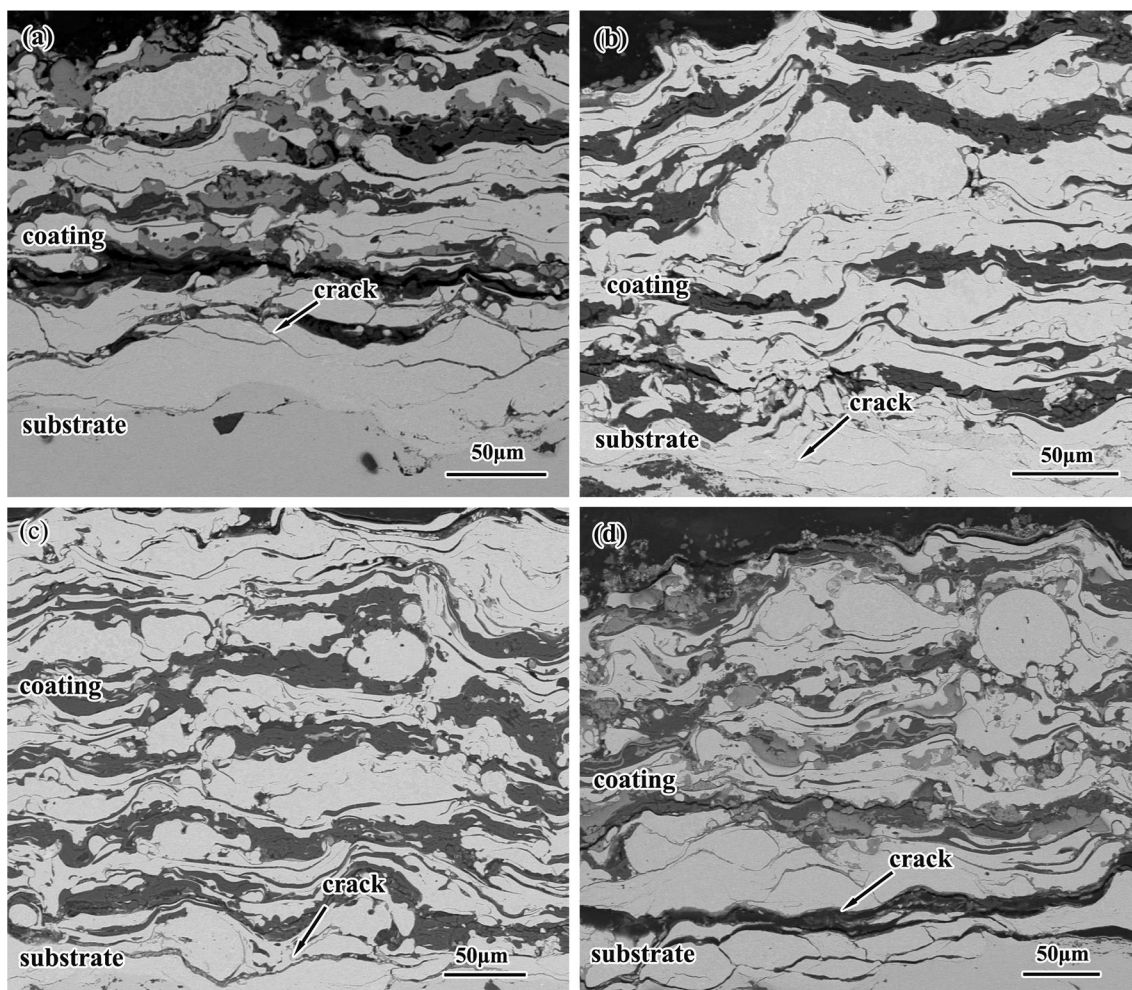
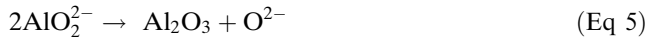


**Fig. 9** Images of cross sections of as-sprayed coatings after corrosion in molten salt at 700 °C (a) C1 after 15 h; (b) C1 after 50 h; (c) C2 after 15 h; (d) C2 after 50 h

the coating, the partial pressure of  $\text{SO}_3$  decreases and the activity of  $\text{Na}_2\text{O}$  increases, then  $\text{Na}_2\text{SO}_4$  shows alkalinity. The  $\text{Al}_2\text{O}_3$  on the surface chemically reacts in alkaline  $\text{Na}_2\text{SO}_4$  as follows:

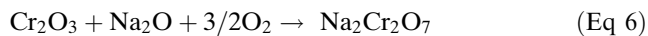


The  $\text{Al}_2\text{O}_3$  film dissolves in this alkaline fusion, and then  $\text{AlO}_2^-$  drifts to the interface between  $\text{Na}_2\text{SO}_4$  and gaseous phase. The counteraction takes place in neutral  $\text{Na}_2\text{SO}_4$ :

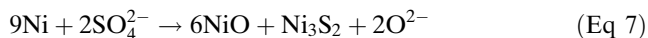


The loose  $\text{Al}_2\text{O}_3$  phase separates out at the interface between  $\text{Na}_2\text{SO}_4$  and gaseous phase. These reactions could make the oxidation film become porous and lose, so the protection film will continue to dissolve and reprecipitate. The performance of  $\text{Al}_2\text{O}_3$  film at high temperature is better than that of  $\text{Cr}_2\text{O}_3$  film, because the diffusion coefficient of metal ions or oxygen ions in the  $\text{Al}_2\text{O}_3$  is smaller than that in the  $\text{Cr}_2\text{O}_3$  by several orders of magnitude. But due to the low density of plasma spraying coating, which has so many defects, such as holes, cracks, when  $\text{Al}_2\text{O}_3$  film is generated, corrosion medium also gets into the inside of coating through defects, which accelerate the degradation of the coating and the consumption of Al. As the corrosion continues, the Al content cannot sustain the growth of  $\text{Al}_2\text{O}_3$ , thus the  $\text{Cr}_2\text{O}_3$  film gets generated instead of  $\text{Al}_2\text{O}_3$  film.

The purpose of Chromium is to improve the hot corrosion resistance of the coating, because the  $\text{Cr}_2\text{O}_3$  has more solubility in neutral  $\text{Na}_2\text{SO}_4$ . When  $\text{Cr}_2\text{O}_3$  and  $\text{Al}_2\text{O}_3$  coexist,  $\text{Cr}_2\text{O}_3$  reacts with  $\text{Na}_2\text{SO}_4$  prior to  $\text{Al}_2\text{O}_3$ . In alkaline fusion,  $\text{Cr}_2\text{O}_3$  reacts as follows:



It is obvious that the alkaline solubility of  $\text{Cr}_2\text{O}_3$  is not only related to the alkaline, but is also related to the oxygen concentration in solution. So the solubility of  $\text{Cr}_2\text{O}_3$  at interface between oxide film and molten salt is less than that between molten salt and air. In molten  $\text{Na}_2\text{SO}_4$ , Ni reacts as follows:



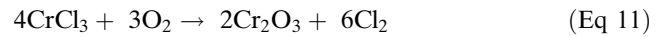
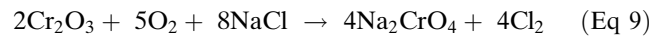
As the reaction continues, the content of  $\text{Cr}_2\text{O}_3$  and NiO increases, then both of them react with each other as follows:



The phase of  $\text{NiCr}_2\text{O}_4$  is generated, whose structure is compact. It can effectively prevent sulfate and oxygen from invading into the coating and improve the corrosion resistance of coating.

NaCl plays an important role in the hot corrosion processes. Some studies have showed that NaCl could destroy the continuity of the surface oxidation film (Ref 29, 30). During the hot corrosion processes, NaCl reaches the substrate through the defects in the oxide film, and then forms the volatile chloride. When gaseous chloride gathers at a certain degree, it results in the cracks or

peeling-offs on the oxide film. The reactions of  $\text{Cr}_2\text{O}_3$  with NaCl are as follows:



The  $\text{Cr}_2\text{O}_3$  film becomes easy to crack and spall in  $\text{Cl}^-$ , then lose the protection (Ref 31). The corrosion resistant of  $\text{Al}_2\text{O}_3$  is good, but its discontinuity and porosity make the diffusion rate of sulfate and oxygen high. When the Al becomes poor, the forming of dense  $\text{Cr}_2\text{O}_3$  delays the diffusion of sulfate and oxygen and the corrosion of oxide layer. Due to more  $\text{Cr}_2\text{O}_3$  in C1 than that in C2 which could be seen in Fig. 7, the hot corrosion resistance of C1 which has more Chromium is better than that of C2.

## 4. Conclusion

Hot corrosion resistances of AlO-CrO/NiCoCrAlYT a and AlO/NiCoCrAlYT a coatings obtained by APS were investigated. The main conclusions can be drawn as follows:

- (1) AlO-CrO/NiCoCrAlYT a and AlO/NiCoCrAlYT a coatings have an uniform microstructure and good bonding to the substrate. The phases of the coating consist of the amorphous phase and several kinds of oxide such as  $\text{Cr}_2\text{O}_3$ ,  $\text{Ni}_3\text{Al}$ , and  $\text{Al}_2\text{O}_3$ . The hardness of AlO-CrO/NiCoCrAlYT a coating is higher than that of AlO/NiCoCrAlYT a coating, while the porosity is lower.
- (2) The hot corrosion resistance of AlO-CrO/NiCoCrAlYT a coating is better than that of AlO/NiCoCrAlYT a coating at both 700 and 900 °C.
- (3) The higher improvement in hot corrosion resistance of the AlO-CrO/NiCoCrAlYT a coating ascribes to lower porosity and more  $\text{Cr}_2\text{O}_3$  which performs better than  $\text{Al}_2\text{O}_3$  in blocking further the inward progress of corrosion and oxidization.

## Acknowledgments

The research was supported by the National 863 plans projects (Grant No. 2012AA03A513) and the National Natural Science Foundation of China (Grant No. 51371044).

## References

1. Y. Zhang, J. Li, J. Huang, and C. Ding, Mechanical and Tribological Properties of Plasma-Sprayed  $\text{Cr}_3\text{C}_2$ -NiCr, WC-Co, and  $\text{Cr}_2\text{O}_3$  Coatings, *J. Therm. Spray Technol.*, 1998, 7(2), p 242-246
2. J. Nicholls and D. Stephenson, High Temperature Coatings for Gas Turbines, *Met. Mater.*, 1991, 7(3), p 156-163





3. W. Brandl, D. Toma, J. Krüger, H. Grabke, and G. Matthäus, The Oxidation Behaviour of HVOF Thermal-Sprayed MCrAlY Coatings, *Surf. Coat. Technol.*, 1997, **94**, p 21-26
4. N. Czech, F. Schmitz, and W. Stamm, Improvement of MCrAlY Coatings by Addition of Rhenium, *Surf. Coat. Technol.*, 1994, **68**, p 17-21
5. G. Goward, Progress in Coatings for Gas Turbine Airfoils, *Surf. Coat. Technol.*, 1998, **108**, p 73-79
6. Q. Wang, Y. Wu, P. Ke, H. Cao, J. Gong, C. Sun, and L. Wen, Hot Corrosion Behavior of AIP NiCoCrAlY (SiB) Coatings on Nickel Base Superalloys, *Surf. Coat. Technol.*, 2004, **186**(3), p 389-397
7. Y. Wu, Q. Wang, P. Ke, C. Sun, J. Gong, F. Wang, and L. Wen, Evaluation of arc ion plated NiCoCrAlYSiB Coatings After Oxidation at 900-1100°C, *Surf. Coat. Technol.*, 2006, **200**(9), p 2857-2863
8. I. Gurrappa, Identification of Hot Corrosion Resistant MCrAlY Based Bond Coatings for Gas Turbine Engine Applications, *Surf. Coat. Technol.*, 2001, **139**(2), p 272-283
9. H. Grünling and R. Bauer, The Role of Silicon in Corrosion-Resistant High Temperature Coatings, *Thin Solid Films*, 1982, **95**(1), p 3-20
10. M. Shirvani and A. Saremi, Nishikata, and T. Tsuru, The Effect of Silicon on Cyclic Oxidation Behavior of Aluminide Coatings on Superalloy IN-738LC, *Mater. Sci. Forum*, 2004, **461-464**, p 335-342
11. J. Vargas, N. Ulion, and J. Goebel, Advanced Coating Development for Industrial/Utility Gas Turbine Engines, *Thin Solid Films*, 1980, **73**(2), p 407-413
12. K. Yang, J. Feng, X. Zhou, and S. Tao, Microstructural Characterization and Strengthening-Toughening Mechanism of Plasma-Sprayed Al<sub>2</sub>O<sub>3</sub>-Cr<sub>2</sub>O<sub>3</sub> Composite Coatings, *J. Therm. Spray Technol.*, 2012, **21**(5), p 1011-1024
13. V.P. Singh, A. Sil, and R. Jayaganthan, Wear of Plasma Sprayed Conventional and Nanostructured Al<sub>2</sub>O<sub>3</sub> and Cr<sub>2</sub>O<sub>3</sub>, Based Coatings, *Trans. Indian Inst. Met.*, 2012, **65**(1), p 1-12
14. Y. Murakami, T. Hirata, and Y. Tsuru, Metastable Phase Relationship in the Al<sub>2</sub>O<sub>3</sub>-Cr<sub>2</sub>O<sub>3</sub> System and Phase Equilibria of 1:1 Composition at 1200 °C, *Nippon Seramikkusu Kyokai Gakujutsu Ronbunshi*, 2002, **110**(6), p 541-543
15. B. Liang and C. Ding, Thermal Shock Resistances of Nanostructured and Conventional Zirconia Coatings Deposited by Atmospheric Plasma Spraying, *Surf. Coat. Technol.*, 2005, **197**(2), p 185-192
16. D. Schwingel, R. Taylor, T. Haubold, J. Wigren, and C. Gualco, Mechanical and Thermophysical Properties of Thick PYSZ Thermal Barrier Coatings: Correlation with Microstructure and Spraying Parameters, *Surf. Coat. Technol.*, 1998, **108**, p 99-106
17. F. Azarmi, J. Saaedi, T.W. Coyle, and J. Mostaghimi, Microstructure Characterization of Alloy 625 Deposited on Nickel Foam Using Air Plasma Spraying, *Adv. Eng. Mater.*, 2008, **10**(5), p 459-465
18. A. Inoue, T. Zhang, and T. Masumoto, Al-La-Ni Amorphous Alloys with a Wide Supercooled Liquid Region, *Mater. Trans. JIM*, 1989, **30**(12), p 965-972
19. A. Miedema, A. Niessen, F. De Boer, R. Boom, and W. Matten, Report, Philips Research Laboratories, Eindhoven, The Netherlands, *Cohesion in Metals: Transition Metals Alloys*, F. De Boer, R. Boom, W. Mattens, A.R. Miedema, and A.K. Niessen, Ed., North-Holland Publishing Co, Amsterdam, 1989,
20. A. Inoue, Y. Shinohara, and J.S. Gook, Thermal and Magnetic Properties of Bulk Fe-Based Glassy Alloys Prepared by Copper Mold Casting, *Mater. Trans. JIM*, 1995, **36**(12), p 1427-1433
21. V. Ponnambalam, S.J. Poon, and G.J. Shiflet, Fe-Based Bulk Metallic Glasses With Diameter Thickness Larger Than One Centimeter, *J. Mater. Res.*, 2004, **19**(05), p 1320-1323
22. J. Cho, S. Zhang, T. Cho, J. Yoon, Y. Joo, and S. Hur, The Processing Optimization and Property Evaluations of HVOF Co-Base Alloy T800 Coating, *J. Mater. Sci.*, 2009, **44**(23), p 6348-6355
23. A. Bradshaw, N. Simms, and J. Nicholls, Hot Corrosion Tests on Corrosion Resistant Coatings Developed for Gas Turbines Burning Biomass and Waste Derived Fuel Gases, *Surf. Coat. Technol.*, 2013, **228**, p 248-257
24. T. Hussain, N. Simms, J. Nicholls, and J. Oakey, Fireside Corrosion Degradation of HVOF Thermal Sprayed FeCrAl Coating at 700-800°C, *Surf. Coat. Technol.*, 2015, **268**, p 165-172
25. C. Zhu, P. Li, A. Javed, G. Liang, and P. Xiao, An Investigation on the Microstructure and Oxidation Behavior of Laser Remelted Air Plasma Sprayed Thermal Barrier Coatings, *Surf. Coat. Technol.*, 2012, **206**(18), p 3739-3746
26. A. Scrivani, U. Bardi, L. Carrafiello, A. Lavacchi, F. Niccolai, and G. Rizzi, A Comparative Study of High Velocity Oxygen Fuel, Vacuum Plasma Spray, and Axial Plasma Spray for the Deposition of CoNiCrAlY Bond Coat Alloy, *J. Therm. Spray Technol.*, 2003, **12**(4), p 504-507
27. S.-G. Tian, X.-D. Lu, T. Wang, and D.-G. Zhu, Influence of Ni-CrAlY Coating on Oxidation Behaviour of Single Crystal Nickel-Based Superalloy, *Trans. Mater. Heat Treat.*, 2011, **32**(11), p 109-116
28. R.L. Jones, Some Aspects of the Hot Corrosion of Thermal Barrier Coatings, *J. Therm. Spray Technol.*, 1997, **6**(1), p 77-84
29. J. Johnson, J. Nicholls, R. Hurst, and P. Hancock, The Mechanical Properties of Surface Scales on Nickel-Base Superalloys—II. Contaminant Corrosion, *Corros. Sci.*, 1978, **18**(6), p 543-553
30. D. McKee, D. Shores, and K. Luthra, The Effect of SO<sub>2</sub> and NaCl on High Temperature Hot Corrosion, *J. Electrochem. Soc.*, 1978, **125**(3), p 411-419
31. Y. Saito, B. Onay, and T. Maruyama, *High Temperature Corrosion of Advanced Materials and Protective Coatings*, Elsevier, Amsterdam, 2012